Geophysical Research Letters

RESEARCH LETTER
10.1029/2019GL082294

Key Points:
- We constrain the density of the north polar ice cap of Mars using gravity and topography data
- We estimate the mean density of the basal unit to be 2007^{-445}_{+493} kg/m^3, suggesting that it may contain more than 50% water ice
- The basal unit may be the largest reservoir of water-ice on Mars after the two polar layered deposits

Supporting Information:
- Supporting Information S1

Correspondence to:
L. Ojha,
luju@jhu.edu

Citation:
Ojha, L., Nerozzi, S., & Lewis, K. (2019). Compositional **c**onstraints on the north polar cap of Mars from **g**ravity and **t**opography. *Geophysical Research Letters*, *46*, 8671–8679. https://doi.org/10.1029/2019GL082294

Received 6 FEB 2019
Accepted 16 MAY 2019
Accepted article online 22 MAY 2019
Published online 1 AUG 2019

©2019. American Geophysical Union. All Rights Reserved.

Compositional Constraints on the North Polar Cap of Mars from Gravity and Topography

Lujendra Ojha[1,2], **Stefano Nerozzi**[3], **and Kevin Lewis**[1]

[1]Department of Earth and Planetary Sciences, The Johns Hopkins University, Baltimore, MD, USA, [2]Department of Earth and Planetary Sciences, Rutgers, The State University of New Jersey, Piscataway, NJ, USA, [3]Institute for Geophysics, Jackson School of Geosciences, The University of Texas at Austin, Austin, TX, USA

Abstract The polar ice caps are the largest reservoir of water ice on Mars. The north polar ice cap is composed of the ice-rich north polar layered deposit (NPLD) and a lower-lying, silicate-rich basal unit (BU). Together, these units represent a record of Martian climate history throughout the Amazonian period. Here we place a bulk compositional constraint on the BU by modeling its gravity signature in both spatial and spectral domains using two independent approaches. We find the density of the BU to be 2007^{-445}_{+493} kg/m^3, suggesting that it may contain 55 $\pm$ 25% water ice. We estimate that the BU contains ~1.5-m global equivalent layer of water making it one of the largest reservoir of water-ice on Mars. Our compositional constraint suggests that the north pole of Mars was not only a cold trap for ices but also an aeolian trap for silicates during the Amazonian period.

Plain Language Summary The north polar cap of Mars consists of thick sheets of extremely pure ice called the north polar layered deposits and the sand-rich basal unit. Radar data have been able to provide information on the composition of the north polar layered deposits; however, the composition of the basal unit is not entirely clear. In this study, we use gravity data of Mars to estimate the density of the basal unit. We find that the density of the basal unit is best matched by a combination of water ice and sand mixture. The relatively low density of the BU suggests that it may contain more than 50% ice. Thus, our study suggests that the basal unit may one of the largest sources of water ice on Mars.

1. Introduction

The north polar ice cap of Mars consists of large, kilometer-thick sheets of water ice that interact with the atmosphere and are thought to record climatic variations in their stratigraphy (Cutts, 1973). The largest section of the north polar ice cap is the topographic dome of Planum Boreum (PB), which is composed of ice-rich north polar layered deposits (NPLD), and an underlying, silicate-rich basal unit (BU; Figure 1). A second lobe of the cap called Gemina Lingula composed entirely of the NPLD is separated from the main dome of PB by a large canyon called Chasma Boreale (Figure 1).

Volumetrically, the NPLD is the second largest reservoir of water ice on the surface of Mars (Brothers et al., 2015; Putzig et al., 2009; Selvans et al., 2010) and plays an important role in regulating the Martian climate via active exchange of water vapor with the atmosphere (e.g., Farmer et al., 1977). The depositional record of ice and sediment in the cap may also contain a record of climatic variations over timescales of 10^5 to 10^7 years (Banks et al., 2010; Cutts, 1973; Herkenhoff & Plaut, 2000; Landis et al., 2016; Pathare et al., 2005). As such, compositional constraints on the Martian polar caps are important for understanding past atmospheric conditions along with global transport cycles of water, sand, and dust on Mars.

The NPLD is composed of subhorizontal layers of ice, up to tens of meters in thickness and makes up the majority of PB volumetrically (>68%; Brothers et al., 2015). The NPLD accumulated throughout its depositional history with various ice-dust fractions (e.g., Cutts & Lewis, 1982; Hvidberg et al., 2012). Radar and gravity data have been used to constrain the bulk composition of the NPLD (e.g., Brothers et al., 2015; Grima et al., 2009; Malin, 1986; Phillips et al., 2008, 2011; Plaut et al., 2007; Selvans et al., 2010). Based on radar data, the NPLD is known to be almost pure ice with a bulk volumetric dust content less than 5% (Grima et al., 2009; Picardi, 2005). Using early gravity data from the Mariner-9 and Viking Orbiter observations, Malin (1986) found the density of the north polar ice cap to be ~1,000 kg/m^3 and estimated the composition to be 5% silicate dust and 95% H_2O-ice.

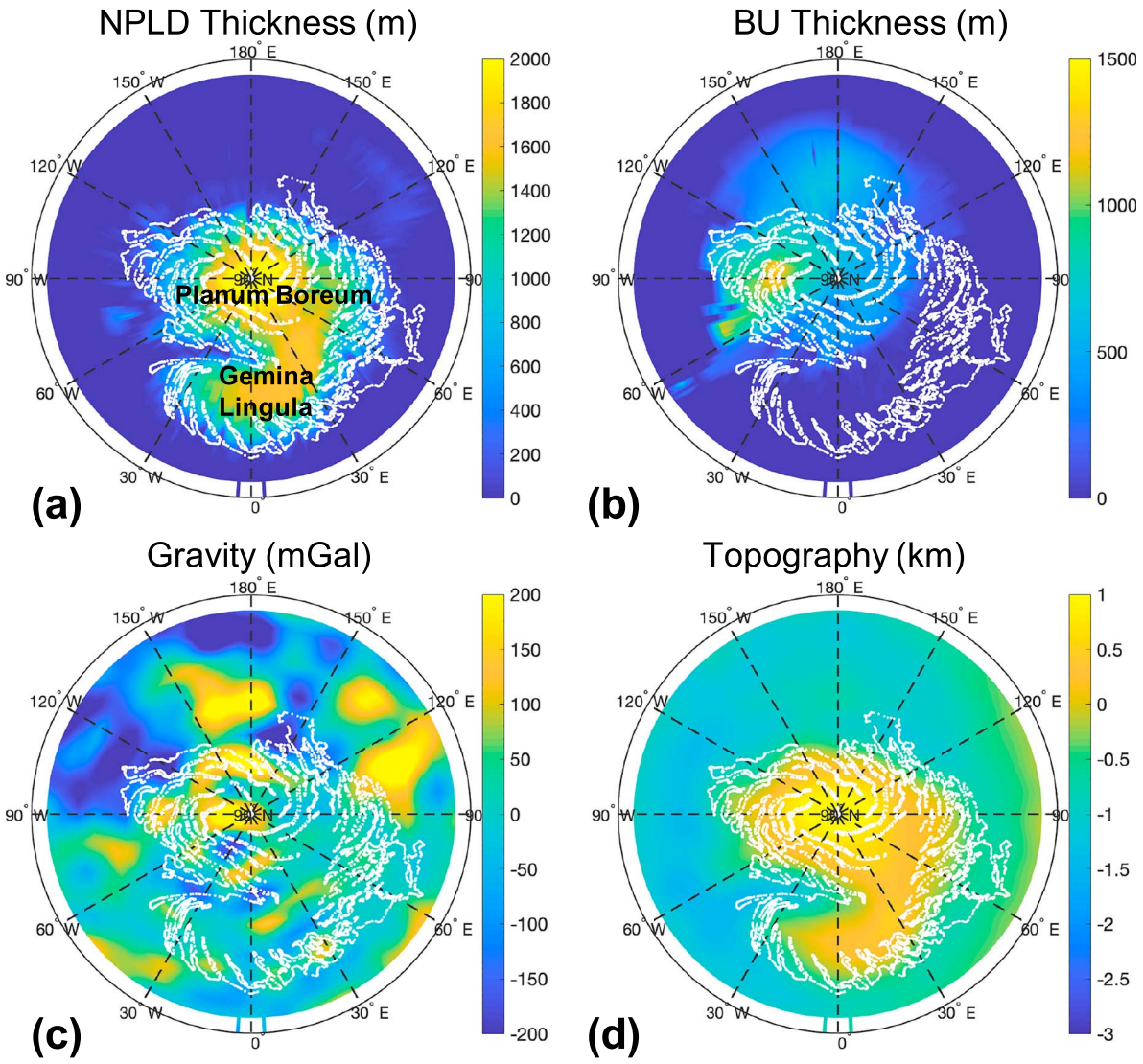

Figure 1. Radar isopach maps showing the thickness of the (a) north polar layered deposit (NPLD) and the (BU) basal unit (BU). (c) Gravity and (d) topography of the north-polar region of Mars. Both gravity and topography fields were expanded to a spherical harmonic degree and order 100. The white outline shows the geographical extent of the north polar ice cap.

While radar and gravity data have been able to provide a compositional constraint on the NPLD, the bulk composition of the underlying BU has been difficult to ascertain. The BU is a low-albedo, sand-rich ice deposit lying stratigraphically between the NPLD, and the underlying Late Hesperian aged Vastitas Borealis Interior Unit (e.g., Brothers et al., 2015; Byrne & Murray, 2002; Fishbaugh & Head, 2005; Malin & Edgett, 2001; Phillips et al., 2008; Selvans et al., 2010; Tanaka et al., 2008). The BU has been further subdivided into two units, the Rupes Tenuis unit and the PB Cavi unit (e.g., Tanaka et al., 2008), separated by a major unconformity. The PB Cavi unit is composed of interbedded icy and lithics-rich layers (Herkenhoff et al., 2007; Tanaka et al., 2008), whereas the Rupes Tenuis unit is more lithic-rich with radar data suggesting the presence of a substantial nonice component within the unit (Plaut et al., 2012). Previous studies based on radar sounding, visible imagery, and spectrometry determined that cavi is composed of sand-sized lithic materials organized in aeolian cross strata and dune forms, weakly cemented by water ice and interbedded with purer ice layers (Byrne & Murray, 2002; Fishbaugh & Head, 2005; Phillips et al., 2008; Selvans et al., 2010; Tanaka et al., 2008). Analysis of MARSIS radar profiles indicates that Rupes is composed mainly of water ice with a lithic component occupying up to 50% of the volume (Plaut et al., 2012; Selvans et al.,

2010). Here we utilize the available Martian gravity and topography data to constrain the bulk density of the north polar ice cap. We then combine the bulk density estimates with previously published radar data to constrain the bulk density and composition of the BU. Although the Rupes and Cavi units are stratigraphically distinct, the current resolution of the Martian gravity data does not permit us to estimate their densities separately.

2. Methods

2.1. Gravity and Topography Admittance

The basic steps we took to estimate the density of the north polar deposits are as follows. We first localized the gravity and topography signature of the north polar ice cap by multiplying the global gravity and topography fields of Mars by a localization window Φ in the spatial domain. The windows are designed to concentrate signals within our area of interest in both space and frequency domains (e.g., Simons et al., 2006). We used the spherical harmonic gravity field of Mars (Konopliv et al., 2016) expanded to degree and order 100, and MOLA topography [MarsTopo719; Wieczorek, 2007] to localize the gravity and topography signature (Figure 1). We localized the gravity and topography signature using spherical localization windows of an angular radius θ with a harmonic bandwidth of L_{win}. We varied θ and L_{win} of the window to ensure that the localized gravity Γ_{lm} and topography Ψ_{lm} estimates had a minimal contribution (<1%) from regions outside of our region of interest. The L_{win} can be increased to ensure that the windowed fields have less than 0.1% contribution from regions outside. However, this leads to a smaller range of spherical harmonic degrees where spectral analyses can take place. The degree l and order m of a spherical harmonic model indicate the scale over which the function varies with latitude and longitude.

We downward continued the localized gravity field to the effective planetary radius, which is given by the following ratio Φ_{00}/h_{00}. Here Φ_{00} and h_{00} are the degree zero terms of the window and the localized topography. We expanded the localized gravity and topography fields in the 4π-normalized spherical harmonic domain and calculated the cross-power spectrum (S) as follows:

$$S_{\Gamma\Psi}(l) = \sum_{m=-l}^{l} \Gamma_{lm}\Psi_{lm}. \tag{1}$$

We estimated the localized admittance $Z(l)$ and the correlation $\gamma(l)$ between gravity and topography as follows:

$$Z(l) = \frac{S_{\Gamma\Psi}(l)}{S_{\Psi\Psi}(l)} \tag{2}$$

and

$$\gamma(\mathrm{l}) = \frac{S_{\Gamma\Psi}(\mathrm{l})}{\sqrt{S_{\Gamma\Gamma}(\mathrm{l})\mathrm{S}_{\Psi\Psi}(\mathrm{l})}}. \tag{3}$$

The admittance function examines the relationship between gravity and topography fields in the spectral domain and allows for the estimation of the load density; however, this approach requires the two fields to be correlated to each other. For this work, we assume that the deflection of the underlying lithosphere in the north polar cap is only due to surface loads. If this assumption is completely valid, then the localized spectral correlation between gravity and topography should have a value of one at all spherical harmonic degrees. The presence of unmodeled signals (related to the noise in the gravity field or subsurface anomalies uncorrelated with the topography) will bias the correlation function downwards but will not bias the admittance spectra (Wieczorek, 2007). In the presence of these unmodeled signals, the correlation spectra will have a value lower than unity, which can be used to estimate the signal:noise (S/N) ratio of the admittance spectrum as follows (*e.g.,* Grott & Wieczorek, 2012; Wieczorek, 2008):

$$\gamma(l) = \left(1 + \frac{1}{S/N(l)}\right)^{\frac{-1}{2}} \tag{4}$$

Wieczorek (2008) used a similar approach as the one described here to estimate the density of the south polar ice cap. Wieczorek (2008) limited his spectral analysis to the range where S/N ratio of the

admittance spectrum exceeded 1.5, noting that due to the loss of fidelity of Martian gravity data with increasing degrees, the magnitude of the correlation and admittance spectra decreases wherever the S/N ratio is less than 1.5. Grott and Wieczorek (2012) also limited their spectral analysis to the range where the S/N ratio exceeded 1.5 to characterize the density and lithospheric structure of Tyrrhena Patera. We find that there are relatively few windows within the geographical boundary of the north polar ice cap with S/N ratio higher than 1.5. Thus, wherever possible, we provide a bulk density estimate from windows where the S/N ratio exceeds 1.5. However, due to the scarcity of such windows in the north pole, we also estimate bulk density from windows where the S/N ratio exceed 1. Previously, we constrained the density of the Medusae Fossae Formation on Mars by analyzing the portion of the admittance spectra with S/N higher than 1 (but less than 1.5) and found the results to be remarkably consistent with radar constraints (Ojha & Lewis, 2018).

The lack of perfect correlation between gravity and topography can also be used to obtain the error ($\sigma(l)$) in the estimate of localized admittance via the following relation:

$$\sigma^2(l) = \frac{S_{\Gamma\Gamma}(l)}{S_{\Psi\Psi}(l)} \frac{1-\gamma^2(l)}{2l} \tag{5}$$

The uncertainty associated with the measurements of the gravity field can also be a notable source of error in the localized admittance. We mostly rely on the Jet Propulsion Laboratory (JPL)-gravity model of Mars (*Konopliv* et al., 2016) for our analysis; however, the associated covariance of the Martian gravity model can be used to generate gravity models that are different from each other but still satisfy the uncertainties. These "clone" gravity models are alternative gravity models than the ones archived in National Aeronautics and Space Administration (NASA)'s Planetary Data System (PDS), but nevertheless completely equivalent because they are from the same statistical data set. We used five different gravity models of Mars to assess how the uncertainty in gravity measurements affects the amplitude of the localized admittance of the north polar ice cap. The localized admittance spectra generated from these five different Mars gravity models were compared with synthetic admittance spectra generated from geophysical models to constrain the bulk density of the north polar ice cap and to estimate the associated uncertainty. We do not rederive the equations for the synthetic admittance spectra in this work (see *Belleguic* et al., 2005; *Wieczorek*, 2008; and *Grott & Wieczorek,* 2012, for the derivation of the synthetic models), but we provide a brief summary and report values of the parameters used in the forward models for reproducibility (Text S1 in the supporting information). Although, we are simultaneously solving for the elastic thickness of the lithosphere (T_e) and the density of the north polar ice cap in our forward models, previous radar work have found that the T_e in the north polar region exceeds 300 km (Phillips et al., 2008*;* Putzig et al., 2009*;* Selvans et al., 2010). We therefore only report best fit load density estimates from models in which the T_e lies between 250 and 300 km.

2.2. Regression Analysis

The density estimates from regional admittance modeling may not be representative of the density of the BU elsewhere. We therefore conducted regression analyses on the gravity and the topography fields of the entire north polar ice cap to estimate the regionally averaged density of the BU. This approach provides an independent estimate of the density of the BU and will allow us to assess the validity of our results from the admittance approach. The radar data do not show a significant deflection of the lithosphere *(Phillips* et al., 2008*; Selvans* et al., 2010) underneath the north polar ice cap; therefore, we assume that the ice cap rests directly on top of a flat crust. In such a scenario, the observed free-air gravity (g_f) is given by

$$g_f = g_b + 2\pi\rho_l G h \tag{6}$$

where g_b is the Bouguer gravity anomaly, ρ_l is the density of the surface load, G is the universal gravitational constant, and h is the thickness of the load. Using our best estimate of the density of the NPLD and the BU from the admittance approach, we perform a Bouguer correction within the geographical boundary of the north polar ice cap. There are large positive and negative Bouguer anomalies within the north polar ice cap, but as will be shown in section 3, over the regional scale, the mean/median Bouguer anomaly is close to zero. Thus, we neglect the g_b in equation (6), in which case g_f is given by

$$g_f = 2\pi G\left(\rho_{\text{npld}} h_{\text{npld}} + \rho_{\text{bu}} h_{\text{bu}}\right) \quad (7)$$

where h is the thickness of the polar units. We use radar-derived thickness estimates of the two polar units (Nerozzi & Holt, 2019) and free-air gravity measurement of the north polar ice cap to solve for the density of the two polar units. To create a gravity and topography grid of the north polar ice cap, we first expanded the spherical harmonic field of Martian gravity to a maximum degree of 100, which yields a global gravity grid of 181 × 361 pixels. We then use the published thickness maps of the NPLD and the BU (e.g., Figure 1) to extract gravity field only from the areas where these two polar units have been mapped. The representation of a spherical field in Cartesian coordinates is inhomogeneous and suffers from meridian convergence and singularities at the poles (e.g., González, 2010). We therefore interpolated the gravity and the topography fields using the Fibonacci lattice, which is a mathematical idealization of natural patterns with equal-area optimal packing. In the Fibonacci lattice, the area represented by each point is nearly identical and help prevents oversampling of points at the poles (Text S2). We ran regression models on the Fibonacci grid representation of the gravity and the thickness of the polar units to estimate the density of the BU (Text S2).

3. Results

3.1. Gravity and Topography Admittance

We found two windows near Chasma Boreale with sufficient gravity-topography correlation (Figure 2; see Figure S1 in the supporting information for examples of location within the North Pole with low correlation). The first window is centered at 85°N, 20°E where we used θ of 7° and L_{win} of 37 to ensure a concentration factor of 99% (Figure 2a). The amplitude of the admittance spectra from five different gravity models vary by less than a few milligals at this location (Figure S2); thus, gravity measurement uncertainty is not a major source of error in our density estimate. Synthetic admittance spectra were compared with the observed admittance spectra from these different gravity models of Mars to constrain the bulk density of the north polar ice cap at this location. The best fit load-density within 1-σ of the observed admittance corresponds to 1,205 $\pm$ 145 kg/m^3 for any T_e greater than 75 km (Fig 2c). However, the T_e in the North Pole is unlikely to be less than 300 km (*Phillips* et al., 2008), so we disregard the density estimates corresponding to the lower T_e values and only report density constraints for an elastic thickness between 250 and 300 km. The best fit load-density within 1-σ of the observed admittance (for the JPL gravity model) for T_e between 250 and 300 km corresponds to 1,100 $\pm$ 40 kg m^{-3} (Figure 2c). The density estimates from the other five gravity models do not vary significantly and yield an averaged bulk density of 1,103 $\pm$ 44 kg/m^3 for the north polar ice cap (Table S1 in the supporting information).

The second window is centered at 84°N, 10°E (Figure 2d), where we used θ of 6° and L_{win} of 39 to localize the gravity and topography signals. Similar to the first location, we generated localized admittance spectra from five different gravity models (Figure S2) and compared them with synthetic admittance spectra to constrain the bulk-density of the north polar cap and associated uncertainty. The best fit load-density within 1-σ of the observed admittance corresponds to 1,220 $\pm$ 130 kg/m^3 for T_e greater than 50 km (Fig 2f). The best fit load-density within 1-σ of the observed admittance (for the JPL gravity model) for T_e between 250 and 300 km corresponds to 1,090 $\pm$ 20 kg/m^3 (Figure 2f). Combining the best fit density estimates from the other five gravity models, we find the average bulk density of the north polar ice cap at this location to be 1,149 $\pm$ 30 kg/m^3 (Table S1).

Although the spatial extents of these two windows slightly overlap, the central locations of the two windows are separated by more than 10° in longitude. The net contribution from the BU to the total thickness of the ice cap varies between the two windows (Text S1 and Figure S3) enabling multiple independent constraints on the density of the BU. Radar permittivity and loss tangent data have shown the ice within the NPLD to be extremely pure (Grima et al., 2009), which suggests that the bulk of the higher density materials required to explain our gravity inferred density is present in the BU. The north polar ice cap has a mean surface temperature of 155 K (Grima et al., 2009), at which, pure H_2O-ice has a density of 930 kg/m^3 (Haynes, 2016). We rely on radar-derived thickness maps of the polar units to compute their mean volumetric contribution within each of the windows (Text S1). Volumetrically, the BU contributes 18% and 16%, respectively, to the total volume of the polar ice cap in the first and the second localization window (Figure S3). Accounting for impurities and assuming the density of the NPLD to be 950 kg/m^3 at most, the bulk average density of the BU that

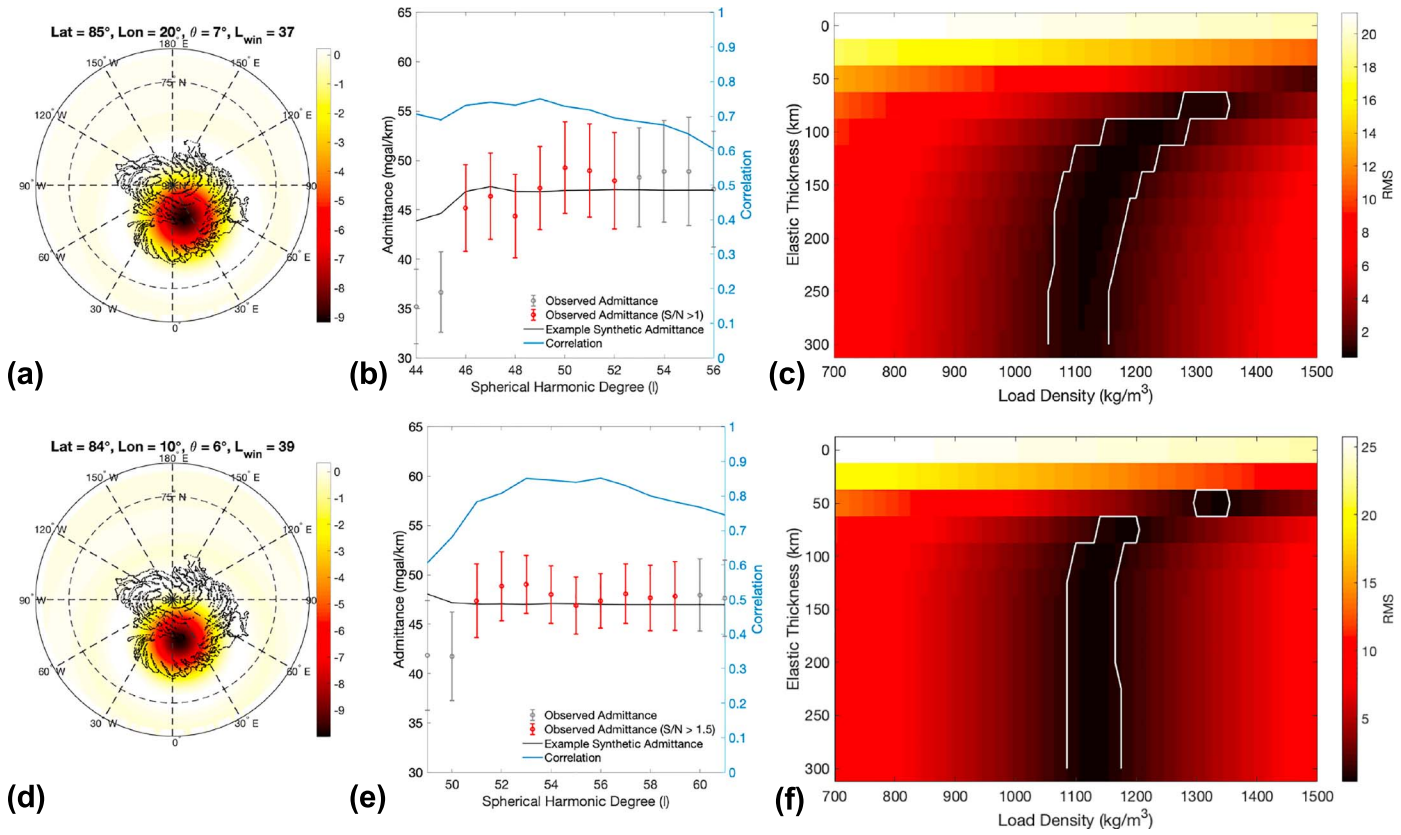

Figure 2. (a) A single taper of L_{win} of 37°, localized within the geographical boundary of the north polar ice cap centered at 85°N and 20°E. The color scale shows the magnitude of the taper. (b) Admittance spectrum and correlation spectrum of the region shown in Figure. 2a. The admittance is plotted in gray where the correlation spectrum is below 0.7 (S/N < 1). The vertical bars show error associated with the admittance estimates. (c) Root-mean-square error between observed and modeled admittances as a function of elastic thickness and load density. The models that fit within the 1-σ error bars of the observed admittance spectrum at each spherical harmonic degrees where S/N exceed 1 are highlighted by the solid white contour. (d) Similar to (a) but centered at 84°N and 10°E and tapered with L_{win} of 39. (e) Similar to (b) but for the region shown in (d). The red bars show admittance estimates where the S/N ratio exceeds 1.5. (f) Same as (c) but for the region shown in (d).

can explain our 1-σ bulk density estimates from the two windows is 1,964 $\pm$ 402 kg/m^3. If the ice within the NPLD is less pure than assumed here, then, our bulk density estimates for the BU may be overestimated.

We also performed multiple linear regression analysis between the observed gravity and the thickness of the NPLD and the BU as an alternative approach to derive their density. The presence of large subsurface gravity anomalies can introduce bias when estimating density using this approach. To ensure that our density estimate from this approach is not significantly impacted by subsurface anomalies, we first perform a Bouguer correction within the north polar ice cap using radar-derived thickness maps and our best fit density estimates of the polar units from admittance analysis. Although there are large positive and negative Bouguer anomalies still present within the north polar ice cap after the Bouguer correction, the mean and the median Bouguer anomalies are -37 and -42 mGal (Figure S4). We perform regression using a linear least squares solver with lower and upper bounds on the density of both the NPLD and BU set to 930 and 3,200 kg/m^3. The best fit density of the NPLD and the BU from regression analysis with lower and upper bounds corresponding to 95% confidence intervals are found to be 1,200 $\pm$ 200 kg/m^3 and 2,050 $\pm$ 450 kg/m^3, respectively (Figure S5).

4. Discussion

Synthetic admittance spectra generated from geophysical models were compared with the observed admittance spectra to constrain the density of the north polar ice cap at two different locations. Based on the joint

constraints from these windows, the north polar ice cap has a bulk density of 1,126 $\pm$ 38 kg/m^3 (Figure 2 and Table S1). It should, however, be emphasized that the bulk density of the north polar ice cap at any given location will vary with the volumetric contribution by the NPLD and BU. Given the known volumetric contribution from the BU at each localization windows (Figure S3), the 1-σ bulk density estimate from the admittance model requires the density of the BU to be 1,964 $\pm$ 402 kg/m^3 (Table S1). We also estimated the density of the north polar ice cap by conducting a regression analysis between the thickness of the polar units and the observed gravity for the entire polar cap. The best fit density of the BU from regression analysis is found to be 2,050 $\pm$ 450 kg/m^3 (Figure S5). The best fit density estimate for the BU from spectral admittance models and spatial regression models are remarkably consistent with each other and yield an average value of 2007^{-445}_{+493} kg/m^3.

There are three major sources of noise and bias in admittance techniques, which can affect our density estimates: (i) uncertainties in the gravity coefficient measurements, (ii) subsurface density anomalies uncorrelated with the topography, and (iii) subsurface density anomalies correlated with the topography (Text S3). In our study area, we find the uncertainties associated with the gravity measurements to have a minor effect on localized admittance and the estimate of the load density (Figure S2 and Table S1). The second source of uncertainty in our density estimate could be from the presence of subsurface anomalies uncorrelated with the topography. It has been previously shown that the uncorrelated subsurface anomalies do not bias the amplitude of the admittance spectrum; however, it can introduce large errors (Text S3). By limiting the comparison between observed and synthetic admittance spectrum to the spherical harmonic domain with S/N higher than 1, we ensure that the errors due to uncorrelated subsurface anomalies do not introduce large uncertainty in our estimates. Lastly, the admittance spectra can have a bias due to the presence of subsurface density anomalies correlated with the topography. In the presence of such signals, the amplitude of the admittance spectrum will have a contribution from both topography and the subsurface anomalies. Consequently, the estimates of the load-density will be overestimated in such a scenario. If such anomalies are present within our localization windows, then our estimate of the density of the BU is an overestimate.

Our average density of the BU suggests that the BU is either composed of a mixture of ice and lithics or lithics with a significant amount of porosity. The exact density of the lithic fraction of the BU is unknown, and here we assume the lithics to be pore-free constituents of Martian meteorites, the density of which generally lies around 3,200 kg/m^3 (Coulson et al., 2007; Neumann et al., 2004). If the BU is completely ice free, then our estimated density of 2007^{-445}_{+493} kg/m^3 requires the porosity in the BU to range between 21 and 51%. On Earth, typical aeolian sand deposits have porosities in the range of 34–40% (Atkins & McBride, 1992; Beard & Weyl, 1973). The overlying NPLD exerts a significant amount of stress on the BU, which will lead to a reduction of pore spaces over a geological time scale. Therefore, it is unlikely for the BU to have pore space exceeding 50%. The BU could have a lower amount of pore space filled by air; however, there are multiple lines of evidence from thermal, neutron spectroscopy, and geological measurements that suggest that the pore space in the BU is most likely occupied by ice. For example, thermal and neutron spectroscopy data have revealed the neighboring Olympia Undae to be ice-cemented aeolian deposit (Feldman et al., 2008; Putzig et al., 2014). The immobility of circumpolar sand dunes in the polar region has been attributed to be due to induration by water (e.g., Bourke et al., 2008; Ewing et al., 2010). Furthermore, recent radar mapping of the BU has found evidence for excess ice within the BU (Nerozzi & Holt, 2019). Thus, the relatively lower density of the BU may be best explained by a mixture of H_2O-ice and lithics.

Assuming the density of H_2O-ice and lithics to be 930 and 3,200 kg/m^3, respectively, our best fit density estimates from admittance approach (1,964 $\pm$ 402 kg/m^3) requires the BU to be composed of 30–80% H_2O ice. Similarly, the best fit density estimate from the regression models (2,050 $\pm$ 450 kg/m^3) requires the BU to be composed of 24—67% water ice. Previously, radar investigations found little attenuation of the radar signal by the BU suggesting that it may only contain a few percent contaminants mixed with water ice (Selvans et al., 2010). Further work by Lauro et al. (2012) and Nerozzi and Holt (2019) have both found evidence for significantly more contaminants in some parts of the BU. Nerozzi and Holt (2019) used SHARAD data to reveal substantial spatial variations in the bulk dielectric constant of the cavi unit in PB and Olympia Planum. The bulk dielectric constant of the BU in Olympia Planum is equivalent to a mixture of 38% basalt and 62% water ice, whereas in the main lobe of PB, water ice is the dominant fraction (~88%) of the BU

(Nerozzi & Holt, 2019). Thus, our constraint on the volume of H_2O ice present in the BU is in agreement with the radar results.

The relatively higher density of the BU compared to the overlying NPLD confirms the findings of previous studies in that the two units have remarkably different compositions (e.g., Brothers et al., 2015; Byrne & Murray, 2002; Fishbaugh & Head, 2005; Malin & Edgett, 2001; Phillips et al., 2008; Selvans et al., 2010; Tanaka et al., 2008). Our density constraint for the BU suggests that unlike the NPLD, the BU has a significant fraction of impurities such as sand and dust-sized particles mixed with H_2O ice. This is in excellent agreement with previously hypothesized formation mechanism of the BU. Tanaka et al. (2008) suggested that the Rupes Tenuis unit could have formed by an episodic accumulation of air fall and wind-blown deposits. Its laterally extensive layers and the overall absence of horizontal mobilization suggest a predominantly vertical construction by atmospheric precipitation and cold-trapping of volatiles, dust, and sand, perhaps forming ice-cemented loess (Tanaka et al., 2008, 2012). Thus, the rupēs unit may be a remnant polar ice deposit that was eroded into the present-day irregular shape, and whose eroded material may have been recycled into the younger cavi unit (Putzig et al., 2009; Tanaka et al., 2008, 2012). The best fit density estimate from localized admittance models suggests that BU could have as much as 59% H_2O ice. Given the current estimate of the volume of the BU of 3.8×10^5 km^3 (Brothers et al., 2015), our density estimate suggests the volume of ice in the BU to exceed 2.2×10^5 km^3 (an ~1.5-m global equivalent layer), similar in magnitude to the volume of ice present in the midlatitude glaciers (~10^5 km^3; Levy et al., 2014). Thus, the BU may be one of the largest reservoirs of water-ice on Mars after the two polar layered deposits. Further, as previously suggested (Tanaka et al., 2008), the density estimate also shows that the north polar region of Mars is not only a cold trap for ices but also an aeolian trap for lithic fines.

5. Conclusion

We conducted a localized admittance study at two different locations within the north polar ice cap to constrain its density. We find the bulk density of the ice cap to be 1,126 $\pm$ 38 kg/m^3. Given the known thickness of the BU within each localization windows, we estimate the required density of the BU required to yield the observed bulk density of the BU and find it to be 1,964 $\pm$ 402 kg/m^3. We also estimate the density of the BU by running a regression model between the thickness of the polar units and the observed free-air gravity anomaly. Using this approach, we find the density of the BU to be 2,050 $\pm$ 450 kg/m^3. Our results suggest the presence of a substantial ice fraction in the BU. Future improvements of the Martian gravity data may allow us to further refine the estimate.

Acknowledgments
The gravity data employed here can be found in the NASA Planetary Data System archive (https://pds.nasa.gov/). The planetary shape model of Mars employed here can be found at (http://www.ipgp.fr/~wieczor/SH/SH.html). The alternative gravity models (clones) are available through the PDS (http://pds-geosciences.wustl.edu/mro/mro-m-rss-5-sdp-v1/mrors_1xxx/extras/clones/). L. O. would like to thank Alison McGraw and Jonathan Bapst whose preliminary review helped improve the scope of the paper. Reviews from Peter James and an anonymous reviewer significantly helped improve the paper.

References

Atkins, J. E., & Mcbride, E. F. (1992). Porosity and packing of Holocene River, Dune, and Beach Sands. *AAPG Bulletin*, *76*.

Banks, M. E., Byrne, S., Galla, K., McEwen, A. S., Bray, V. J., Dundas, C. M., et al. (2010). Crater population and resurfacing of the Martian north polar layered deposits. *Journal of Geophysical Research*, *115*, E08006. https://doi.org/10.1029/2009JE003523

Beard, D. C., & Weyl, P. K. (1973). Influence of texture on porosity and permeability of unconsolidated sand. *American Association of Petroleum Geologists Bulletin*, *57*.

Belleguic, V., Lognonne, P., & Wieczorek, M. (2005). Constraints on the Martian lithosphere from gravity and topography data. *Journal of Geophysical Research*, *110*, E11005. https://doi.org/10.1029/2005JE002437

Bourke, M. C., Edgett, K. S., & Cantor, B. A. (2008). Recent aeolian dune change on Mars. *Geomorphology*, *94*(1), 247–255. https://doi.org/10.1016/j.geomorph.2007.05.012

Brothers, T. C., Holt, J. W., & Spiga, A. (2015). Planum Boreum basal unit topography, Mars: Irregularities and insights from SHARAD. *Journal of Geophysical Research: Planets*, *120*, 1357–1375. https://doi.org/10.1002/2015JE004830

Byrne, S., & Murray, B. (2002). North polar stratigraphy and the paleo-erg of Mars. *Journal of Geophysical Research*, *107*(E6), 5044. https://doi.org/10.1029/2001JE001615

Coulson, I. M., Beech, M., & Nie, W. (2007). Physical properties of Martian meteorites: Porosity and density measurements. *Meteoritics and Planetary Science*, *42*(12), 2043–2054. https://doi.org/10.1111/j.1945-5100.2007.tb01006.x

Cutts, J. A. (1973). Nature and origin of layered deposits of the Martian polar regions. *Journal of Geophysical Research*, *78*(20), 4231–4249. https://doi.org/10.1029/JB078I020P04231

Cutts, J. A., & Lewis, B. H. (1982). Models of climate cycles recorded in Martian polar layered deposits. *Icarus*, *50*(2–3), 216–244. https://doi.org/10.1016/0019-1035(82)90124-5

Ewing, R. C., Peyret, A.-P. B., Kocurek, G., & Bourke, M. (2010). Dune field pattern formation and recent transporting winds in the Olympia Undae Dune Field, north polar region of Mars. *Journal of Geophysical Research*, *115*, E08005. https://doi.org/10.1029/2009JE003526

Farmer, C. B., Davies, D. W., Holland, A. L., Laporte, D. D., & Doms, P. E. (1977). Mars: Water vapor observations from the Viking orbiters. *Journal of Geophysical Research*, *82*(28), 4225–4248. https://doi.org/10.1029/JS082i028p04225

Feldman, W., Bourke, M., Elphic, R., Maurice, S., Bandfield, J., Prettyman, T., et al. (2008). Hydrogen content of sand dunes within Olympia Undae. *Icarus*, *196*(2), 422–432. https://doi.org/10.1016/j.icarus.2007.08.044

Fishbaugh, K. E., & Head, J. W. (2005). Origin and characteristics of the Mars north polar basal unit and implications for polar geologic history. *Icarus*, *174*, 444–474. https://doi.org/10.1016/j.icarus.2004.06.021

González, Á. (2010). Measurement of areas on a sphere using Fibonacci and latitude-longitude lattices. *Mathematical Geosciences*, *42*(1), 49–64. https://doi.org/10.1007/s11004-009-9257-x

Grima, C., Kofman, W., Mouginot, J., Phillips, R. J., Hérique, A., Biccari, D., et al. (2009). North polar deposits of Mars: Extreme purity of the water ice. *Geophysical Research Letters*, *36*, L03203. https://doi.org/10.1029/2008GL036326

Grott, M., & Wieczorek, M. A. (2012). Density and lithospheric structure at Tyrrhena Patera, Mars, from gravity and topography data. *Icarus*, *221*(1), 43–52. https://doi.org/10.1016/j.icarus.2012.07.008

Haynes, W. M. (2016). *Hdbk chemistry and physics*. CRC Press.

Herkenhoff, K. E., Byrne, S., Russell, P. S., Fishbaugh, K. E., & McEwen, A. S. (2007). Meter-scale morphology of the north polar region of Mars. *Science*, *317*(5845), 1711. https://doi.org/10.1126/science.1143544

Herkenhoff, K. E., & Plaut, J. J. (2000). Surface ages and resurfacing rates of the polar layered deposits on Mars. *Icarus*, *144*(2), 243–253. https://doi.org/10.1006/icar.1999.6287

Hvidberg, C. S., Fishbaugh, K. E., Winstrup, M., Svensson, A., Byrne, S., & Herkenhoff, K. E. (2012). Reading the climate record of the Martian polar layered deposits. *Icarus*, *221*(1), 405–419. https://doi.org/10.1016/j.icarus.2012.08.009

Konopliv, A. S., Park, R. S., & Folkner, W. M. (2016). An improved JPL Mars gravity field and orientation from Mars orbiter and lander tracking data. *Icarus*, *274*, 253–260. https://doi.org/10.1016/j.icarus.2016.02.052

Landis, M. E., Byrne, S., Daubar, I. J., Herkenhoff, K. E., & Dundas, C. M. (2016). A revised surface age for the north polar layered deposits of Mars. *Geophysical Research Letters*, *43*, 3060–3068. https://doi.org/10.1002/2016GL068434

Lauro, S. E., Mattei, E., Soldovieri, F., Pettinelli, E., Orosei, R., & Vannaroni, G. (2012). Dielectric constant estimation of the uppermost basal unit layer in the Martian Boreales Scopuli region. *Icarus*, *219*(1), 458–467. https://doi.org/10.1016/j.icarus.2012.03.011

Levy, J. S., Fassett, C. I., Head, J. W., Schwartz, C., & Watters, J. L. (2014). Sequestered glacial ice contribution to the global Martian water budget: Geometric constraints on the volume of remnant, midlatitude debris-covered glaciers. *Journal of Geophysical Research: Planets*, *119*, 2188–2196. https://doi.org/10.1002/2014JE004685

Malin, M. C. (1986). Density of Martian north polar layered deposits: Implications for composition. *Geophysical Research Letters*, *13*(5), 444–447. https://doi.org/10.1029/GL013i005p00444

Malin, M. C., & Edgett, K. S. (2001). Mars Global Surveyor Mars Orbiter Camera: Interplanetary cruise through primary mission. *Journal of Geophysical Research*, *106*(E10), 23,429–23,570. https://doi.org/10.1029/2000JE001455

Nerozzi, S., & Holt, J. W. (2019). Buried ice and sand caps at the north pole of Mars: revealing a record of climate change in the cavi unit with SHARAD. *Geophysical Research Letters*, *46*, 7278–7286. https://doi.org/10.1029/2019GL082114

Neumann, G. A., Zuber, M. T., Wieczorek, M. A., McGovern, P. J., Lemoine, F. G., & Smith, D. E. (2004). Crustal structure of Mars from gravity and topography. *Journal of Geophysical Research*, *109*, E08002. https://doi.org/10.1029/2004JE002262

Ojha, L., & Lewis, K. (2018). The density of the Medusae Fossae Formation: Implications for its composition, origin, and importance in Martian history. *Journal of Geophysical Research: Planets*, *123*, 1368–1379. https://doi.org/10.1029/2018JE005565

Pathare, A. V., Paige, D. A., & Turtle, E. (2005). Viscous relaxation of craters within the Martian south polar layered deposits. *Icarus*, *174*(2 SPEC. ISS), 396–418. https://doi.org/10.1016/j.icarus.2004.10.031

Phillips, R. J., Davis, B. J., Tanaka, K. L., Byrne, S., Mellon, M. T., Putzig, N. E., et al. (2011). Massive CO_2 ice deposits sequestered in the south polar layered deposits of Mars. *Science*, *332*(6031), 838–841. https://doi.org/10.1126/science.1203091

Phillips, R. J., Zuber, M. T., Smrekar, S. E., Mellon, M. T., Head, J. W., Tanaka, K. L., et al. (2008). Mars north polar deposits: Stratigraphy, age, and geodynamical response. *Science*, *320*(5880), 1182–1185. https://doi.org/10.1126/science.1157546

Picardi, G. (2005). Radar soundings of the subsurface of Mars. *Science*, *310*(5756), 1925–1928. https://doi.org/10.1126/science.1122165

Plaut, J. J., Frigeri, A., & Orosei, R. (2012). Compositional constraints on the Martian north polar basal unit from MARSIS radar sounding data. In Lunar and science conference (Vol. 43).

Plaut, J. J., Picardi, G., Safaeinili, A., Ivanov, A. B., Milkovich, S. M., Cicchetti, A., et al. (2007). Subsurface radar sounding of the south polar layered deposits of Mars. *Science*, *316*(5821), 92–95. https://doi.org/10.1126/science.1139672

Putzig, N. E., Mellon, M. T., Herkenhoff, K. E., Phillips, R. J., Davis, B. J., Ewer, K. J., & Bowers, L. M. (2014). Thermal behavior and ice-table depth within the north polar erg of Mars. *Icarus*, *230*, 64–76. https://doi.org/10.1016/j.icarus.2013.07.010

Putzig, N. E., Phillips, R. J., Campbell, B. A., Holt, J. W., Plaut, J. J., Carter, L. M., et al. (2009). Subsurface structure of Planum Boreum from Mars Reconnaissance Orbiter Shallow Radar soundings. *Icarus*, *204*(2), 443–457. https://doi.org/10.1016/j.icarus.2009.07.034

Selvans, M. M., Plaut, J. J., Aharonson, O., & Safaeinili, A. (2010). Internal structure of Planum Boreum, from Mars advanced radar for subsurface and ionospheric sounding data. *Journal of Geophysical Research*, *115*, E09003. https://doi.org/10.1029/2009JE003537

Simons, F. J., Dahlen, F. A., & Wieczorek, M. A. (2006). Spatiospectral concentration on a sphere. *SIAM Review*, *48*(3), 504–536.

Tanaka, K., Rodriguez, J., Skinner, J., Bourke, M., Fortezzo, C., Herkenhoff, K., et al. (2008). North polar region of Mars: Advances in stratigraphy, structure, and erosional modification. *Icarus*, *196*(2), 318–358. https://doi.org/10.1016/j.icarus.2008.01.021

Tanaka, K. L., Fortezzo, C. M., & Ryan, D. A. (2012). Geologic map of the north polar region of Mars. US Department of the Interior, US Geological Survey.

Wieczorek, M. A. (2007). Gravity and topography of the terrestrial planets. In *Treatise on Geophysics*, (Vol. 10, pp. 165–206). https://doi.org/10.1016/B978-044452748-6.00156-5

Wieczorek, M. A. (2008). Constraints on the composition of the Martian south polar cap from gravity and topography. *Icarus*, *196*(2), 506–517. https://doi.org/10.1016/j.icarus.2007.10.026